

Highly Tunable Hybrid Quantum Dots with Charge Detection

C. Rössler,^{1, a)} B. Küng,¹ S. Dröscher,¹ T. Choi,¹ T. Ihn,¹ K. Ensslin,¹ and M. Beck²

¹⁾ *Solid State Physics Laboratory, ETH Zurich, 8093 Zurich, Switzerland*

²⁾ *Institute for Quantum Electronics, ETH Zurich, 8093 Zurich, Switzerland*

(Dated: 15 September 2010)

In order to employ solid state quantum dots as qubits, both a high degree of control over the confinement potential as well as sensitive charge detection are essential. We demonstrate that by combining local anodic oxidation with local Schottky-gates, these criteria are nicely fulfilled in the resulting hybrid device. To this end, a quantum dot with adjacent charge detector is defined. After tuning the quantum dot to contain only a single electron, we are able to observe the charge detector signal of the quantum dot state for a wide range of tunnel couplings.

PACS numbers: 73.63.Kv, 73.63.Nm, 73.23.Hk

Keywords: Quantum Dot, Local Anodic Oxidation, Charge Readout, Single Electron

Quantum dots (QDs) are a playground for quantum engineered devices, since many system properties like tunnel coupling, energy spacing, etc. can be controlled and varied. In particular, electrostatically defined quantum dots, created by local depletion of a two-dimensional electron gas (2DEG) in an $\text{Al}_x\text{Ga}_{1-x}\text{As}$ heterostructure, allow to build charge- and spin-qubits^{1,2}. To this end, both a high degree of tunability of the confinement potential as well as the capability to sense the charge state of the QD are needed. By employing Schottky-split-gates it is possible to tune the local electrostatic potential in a way that only one electron is left in the QD³. Measuring the conductance of a nearby quantum point contact (QPC) facilitates to determine the charge state of the QD even if no measurable current flows through the QD⁴. However, electrostatic screening of metal gates between QD and QPC strongly decreases the readout fidelity as compared to fabrication techniques without metal gates, like etching or local anodic oxidation (LAO)⁵. But the latter fabrication techniques have the disadvantage of a low tunability because the confinement potential is pre-defined after fabrication. Tackling this issue by employing a patterned top gate appears to sacrifice the readout capabilities of LAO defined QDs⁶. The combination of local Schottky-gates with LAO promises to combine highly tunable confinement potentials with good detector readout fidelity.

The fabrication is carried out on an $\text{Al}_x\text{Ga}_{1-x}\text{As}$ heterostructure. The 2DEG resides at the heterointerface, $z \approx 40$ nm beneath the surface. The 2DEG's sheet density is $n_S = 4.9 \times 10^{15} \text{ m}^{-2}$ with a Drude mobility of $\mu = 33 \text{ m}^2/\text{Vs}$, as determined in Van-der-Pauw geometry at a temperature of $T = 4.2 \text{ K}$. After defining the 2DEG mesa and the outer gate leads via optical lithography (not shown), 30 nm thick Ti/Au gates are deposited via e-beam lithography (yellow areas in Fig. 1). An atomic force microscope (AFM) is used to record a topographic image of the sample's surface. By applying a voltage

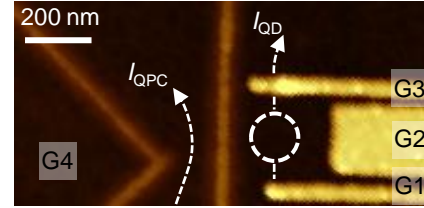


FIG. 1. (color online) AFM micrograph of the sample surface (black). The vertical and diagonal oxide lines are 10 nm high and define a QPC in the underlying 2DEG. The 2DEG area labeled G4 on the left hand side is used to capacitively control the current through the QPC. Applying voltages to the 30 nm thick Schottky gates G1, G2 and G3 (yellow) defines a QD.

$V_{\text{TIP}} \sim -30 \text{ V}$ to the AFM tip at ambient conditions, the heterostructure is locally oxidized and the underlying 2DEG is depleted⁷. Writing oxide lines (vertical and diagonal lines in Fig. 1) left of the QD-gates defines a QPC. In a pioneering work on combining Schottky-gates with LAO⁸, the e-beam lithography was done after LAO. Hence, the alignment had to be done by e-beam lithography with respect to pre-defined markers, limiting the accuracy to $\Delta x \sim 50 \text{ nm}$ ⁸. We find that the accuracy of positioning the oxide line is limited by the AFM lithography step to $\Delta x \sim 10 \text{ nm}$ and can easily be compensated in the experiment by applying appropriate voltages to the gates. On the right side of the central oxide line a QD (white dashed circle in Fig. 1) is defined between gates G1, G2, G3 and the oxide line.

Applying voltages $V \lesssim -0.6 \text{ V}$ leads to increased switching noise which is typical for shallow 2DEG's because of the small tunnel barriers in growth-direction. This experimental limitation can be overcome by adjusting the pinch-off voltages of the gates to values close to $V = 0$. Applying positive gate-voltages during cooldown⁹ should create a depleting (negative) potential once the gates are set to zero at low temperature. It turns out that this so called pre-biased cooldown works very well on the shallow-2DEG structure employed here. Additionally a bias $V_{2\text{DEG}}$ can be applied to the QPC-circuit

^{a)} Electronic mail: roessler@phys.ethz.ch

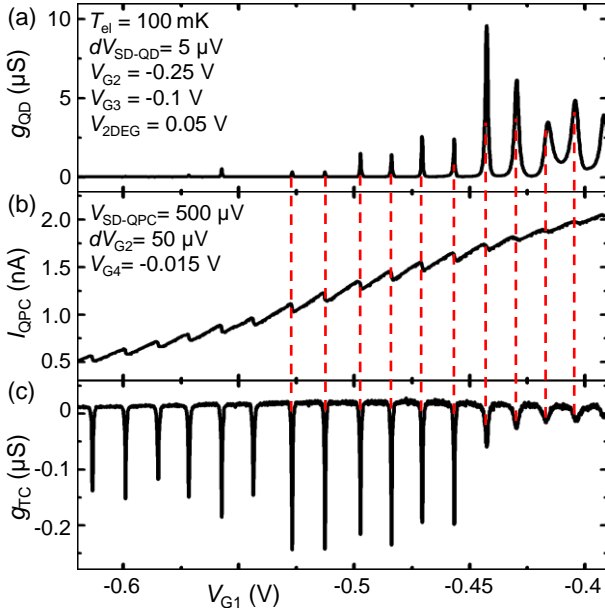


FIG. 2. (a) Differential conductance of the QD g_{QD} , plotted as a function of gate voltage V_{G1} . Maxima in g_{QD} are Coulomb oscillations. For gate voltages $V_{G1} < -0.57$ V (left), no more Coulomb oscillations are observed. (b) Current through the QPC I_{QPC} , plotted for the same gate voltages. Kinks in I_{QPC} are caused by a change of the QD occupancy by one electron. (c) Transconductance $g_{TC} = dI_{QPC}/dV_{G2}$, measured by modulating voltage V_{G2} and detecting dI_{QPC} with lock-in technique. Local minima reflect the charge occupancy of the QD.

with respect to the QD-circuit, thereby acting as an in-plane-gate.

The source-drain current of both circuits is measured at an electron temperature of $T_{el} \approx 100$ mK as a function of the voltages applied to the Schottky gates. Figure 2(a) shows the differential conductance g_{QD} of the QD-circuit, measured with lock-in technique as a function of the voltage applied to gate G1. Oscillations in g_{QD} indicate that a QD is defined between the central oxide line and gates G1, G2 and G3, as sketched in Fig. 1. Since gate G1 also defines one tunnel barrier of the QD, the amplitude of the Coulomb oscillations decreases rapidly until no measurable current flows for $V_{G1} < -0.6$ V. The simultaneously measured current I_{QPC} through the QPC is shown in Fig. 2(b). Stepping V_{G1} to lower values decreases I_{QPC} due to capacitive crosstalk between the gate and the QPC. On top of that, I_{QPC} increases step-like when the occupancy of the QD changes by one electron. Vertical dashed lines emphasize that the steps in I_{QPC} coincide with maxima in g_{QD} . Moreover, the QPC is still sensitive to the charge state of the QD when g_{QD} becomes unmeasurably small. The step height in Fig. 2(b) is $\Delta I_{QPC}/I_{QPC} \approx 10\%$ at $V_{G1} \approx -0.5$ V. We find step heights of 5% for strongly coupled QDs and 15% when detecting charging events of double QDs (not shown). This indicates screening via nearby electrons in the 2DEG

Technique:	Schottky	Hybrid	Oxidation
$\Delta I_{QPC}/I_{QPC} :$	1...2 %	5...15 %	5...40 %

TABLE I. QPC read-out efficiency $\Delta I_{QPC}/I_{QPC}$ of QDs fabricated by different methods. Values obtained from^{4,5,10,11}.

which is reduced when depleting large areas in order to define a double QD. Table I shows typical readout efficiencies of QDs fabricated by different methods. The step height of the hybrid structures lies in between typical values of purely Schottky- and purely AFM-defined QDs, with the spread being due to different sample geometries and QPC pinch-off slopes.

Figure 2(c) shows the transconductance $g_{TC} = dI_{QPC}/dV_{G2}$ measured by modulating the voltage V_{G2} and detecting dI_{QPC} with lock-in technique. The transconductance minima directly represent the charge occupancy of the QD^{10,12}. As expected, the peak shape of transconductance minima and Coulomb oscillations are identical when the QD is weakly coupled to the leads. In contrast, the peak shape shows clear deviations in the case of strong coupling. For example, the rightmost three Coulomb peaks are asymmetric in direct transport, but symmetric in the transconductance dip. This deviation has to our knowledge not been observed before in direct transport and demonstrates the high fidelity of our detector readout.

In order to explore the tunability of our scheme, another sample with similar geometry is tuned to a very asymmetric configuration where it is only coupled to the 2DEG underneath gate G1 ($V_{G1} > -0.3$ V, $V_{G2} < -0.8$ V, $V_{G3} = -2$ V). Fig. 3 shows g_{TC} , plotted in false colors as a function of V_{G1} and V_{G2} . The transconductance is finite and positive throughout the whole parameter range, indicating that the QPC is neither pinched off nor insensitive to changes in the local electrostatic potential. Single resonances with different slopes (marked by black arrows) are caused by trapped states in the environment, most likely in the doping layer or in the oxide line. A series of Coulomb resonances (white arrows) exhibits the same slope of $\Delta V_{G1}/\Delta V_{G2} \approx 4$, indicating that they correspond to charging events of the same QD. Moreover, the stronger coupling of gate G1 as compared to G2 confirms that the QD has been "pushed" away from gates G2 and G3, towards the oxide line and gate G1. Each QD resonance is characterized by an abrupt end at very negative V_{G1} (bottom) and a washed out regime for less negative V_{G1} (top). This observation is expected from the sample's design, where gate G1 controls the height of the tunnel barrier between QD and 2DEG. Making V_{G1} more negative and therefore increasing the tunnel barrier reduces the tunnel rate between QD and 2DEG until it is comparable to the gate modulation frequency of $f_{LI} = 193$ Hz and the QD can not compensate the gate modulation by electron tunnelling. The full width at half maximum FWHM ≈ 1 meV of the dips in g_{TC} is dominated by the modulation amplitude dV_{G2} . For smaller tunnel barriers, the leftmost two resonances start

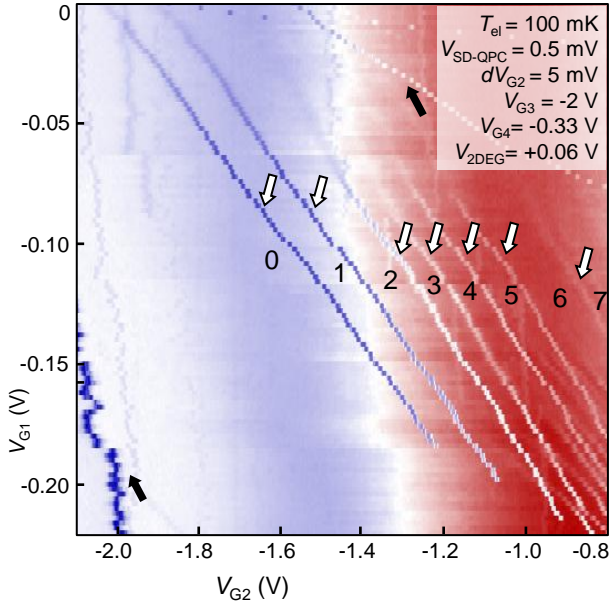


FIG. 3. (color online) Transconductance $g_{TC} = dI_{QPC}/dV_{G2}$ in false colors from $g_{TC} = 2 \times 10^{-9} \text{ S}$ (blue) to $g_{TC} = 12 \times 10^{-9} \text{ S}$ (red), plotted as a function of V_{G1} and V_{G2} . Local minima are caused by Coulomb resonance of the QD (white arrows) or trapped states in the environment (black arrows). Between the QD resonances, the electron number is fixed (labeled from 0 to 7).

to broaden at gate voltages of $V_{G1} \gtrsim -0.08 \text{ V}$. This observation indicates that due to the reduced tunnel barrier height, the tunnel broadening exceeds 1 meV , which corresponds to a tunnel rate of $\Gamma = \text{FWHM}/h \gtrsim 2 \times 10^{11} \text{ Hz}$. Taking these two values of the tunnel barrier as references, we can estimate the coefficient relating top gate voltage and tunnel rate to be of the order of 12 mV per decade. This is in good agreement with tunnel rate measurements on QDs with a comparable Schottky-gate layout¹³.

Observing each QD state over a wide range of tunnel couplings strongly indicates that after the leftmost QD resonance, the QD is completely emptied of electrons. This enables us to label the number of electrons on the QD ("0" to "7" in Fig. 3). The charging energy of the first two electrons of $E_C \sim 10 \text{ meV}$ (determined from the slope $\Delta E/\Delta V_{G2} = 0.5 \times \Delta V_{SD}/\Delta V_{G2}$) is among the largest values reported for laterally defined QDs. Strikingly, the addition energy of the electronic states labeled 2 and 6 is slightly larger than the adjacent addition energies. These "magic numbers" are expected from a two-dimensional confinement potential and have already been discussed in transport experiments on QDs^{3,14}. Moreover, the tunnel broadening of the first two electronic states sets in at $V_{G1} \sim -0.08 \text{ V}$, whereas the following four QD states begin to broaden at $V_{G1} \sim -0.11 \text{ V}$. Observing the same tunnel broadening for different tunnel barrier heights indicates different tunnel rates of the involved orbital states. Again, the observation of tunnel

broadened states of a few-electron QD in the QPC signal demonstrates the capabilities of the presented device.

In conclusion, we fabricated a QD with adjacent QPC by combining Schottky-gates with local anodic oxidation. The resulting hybrid device combines the advantages of both techniques. Reduced screening of the charge detector facilitates good charge readout and the employed Schottky-gates demonstrate high tunability of the QD. Tuning the QD to the few-electron regime, we can detect these charge states over a range of more than nine orders of tunnel coupling. Signatures of shell filling effects are observed both in the excitation energy and in the tunnel rate. Further improvement of the device geometry and the extension to few-electron double QDs promises devices with very desirable properties in view of defining solid state qubits.

We acknowledge the support of the ETH FIRST laboratory and financial support of the Swiss Science Foundation (Schweizerischer Nationalfonds, NCCR Nanoscience).

REFERENCES

- ¹T. Hayashi, T. Fujisawa, H. D. Cheong, Y. H. Jeong, and Y. Hirayama, *Phys. Rev. Lett.* **91**, 22 (2003)
- ²J. R. Petta, A. C. Johnson, J. M. Taylor, E. A. Laird, A. Yacoby, M. D. Lukin, C. M. Marcus, M. P. Hanson, and A. C. Gossard, *Science* **309**, 2180 (2005)
- ³M. Ciorga, A. S. Sachrajda, P. Hawrylak, C. Gould, P. Zawadzki, S. Jullian, Y. Feng, and Z. Wasilewski, *Phys. Rev. B* **61**, 16315 (2000)
- ⁴M. Field, C. G. Smith, M. Pepper, D. A. Ritchie, J. E. F. Frost, G. A. C. Jones, and D. G. Hasko, *Phys. Rev. Lett.* **70**, 1311 (1993)
- ⁵See for example S. Gustavsson, R. Leturcq, T. Ihn, K. Ensslin, and A. C. Gossard, *Electrons in quantum dots - One by one*, J. Appl. Phys. **105**, 122401 (2009)
- ⁶M. Sigrist, S. Gustavsson, T. Ihn, K. Ensslin, D. Driscoll, A. Gossard, M. Reinwald, and W. Wegscheider, *Physica E* **32**, 5-8 (2006)
- ⁷R. Held, T. Vancura, T. Heinzel, K. Ensslin, M. Holland, and W. Wegscheider, *Appl. Phys. Lett.* **73**, 262 (1998)
- ⁸M. C. Rogge, C. Fühner, U. F. Keyser, R. J. Haug, M. Bichler, G. Abstreiter, and W. Wegscheider, *Appl. Phys. Lett.* **83**, 6 (2003)
- ⁹M. Pioro-Ladriere, J. H. Davies, A. R. Long, A. S. Sachrajda, L. Gaudreau, P. Zawadzki, J. Lapointe, J. Gupta, Z. Wasilewski, and S. Studenikin, *Phys. Rev. B* **72**, 115331 (2005)
- ¹⁰J. M. Elzerman, R. Hanson, J. S. Greidanus, L. H. Willems van Beveren, S. De Franceschi, L. M. K. Vandersypen, S. Tarucha, and L. P. Kouwenhoven, *Phys. Rev. B* **67**, 161308(R) (2003)
- ¹¹S. Gustavsson, R. Leturcq, B. Simovic, R. Schleser, T. Ihn, P. Studerus, K. Ensslin, D. C. Driscoll, and A. C. Gossard, *Phys. Rev. Lett.* **96**, 076605 (2006)
- ¹²R. Schleser, E. Ruth, T. Ihn, K. Ensslin, D. C. Driscoll, and A. C. Gossard, *Appl. Phys. Lett.* **85**, 11 (2004)
- ¹³T. Ota, T. Hayashi, K. Muraki, and T. Fujisawa, *Appl. Phys. Lett.* **96**, 032104 (2010)
- ¹⁴S. Tarucha, D. G. Austing, T. Honda, R. J. van der Hage, and L. P. Kouwenhoven, *Phys. Rev. Lett.* **77**, 3613 (1996)
- ¹⁵R. Hanson, L. H. Willems van Beveren, I. T. Vink, J. M. Elzerman, W. J. M. Naber, F. H. L. Koppens, L. P. Kouwenhoven, and L. M. K. Vandersypen, *Phys. Rev. Lett.* **94**, 196802 (2005)